Environmental Science & Technology

pubs.acs.org/est

Article

Comparison of Mobile and Fixed-Site Black Carbon Measurements for High-Resolution Urban Pollution Mapping

Sarah E. Chambliss, Chelsea V. Preble, Julien J. Caubel, Troy Cados, Kyle P. Messier, Ramón A. Alvarez, Brian LaFranchi, Melissa Lunden, Julian D. Marshall, Adam A. Szpiro, Thomas W. Kirchstetter, and Joshua S. Apte*

Cite This: *Environ. Sci. Technol.* 2020, 54, 7848−7857

Read Online

ACCESS | Metrics & More | Article Recommendations | Supporting Information

ABSTRACT: Urban concentrations of black carbon (BC) and other primary pollutants vary on small spatial scales (<100m). Mobile air pollution measurements can provide information on fine-scale spatial variation, thereby informing exposure assessment and mitigation efforts. However, the temporal sparsity of these measurements presents a challenge for estimating representative long-term concentrations. We evaluate the capabilities of mobile monitoring in the represention of time-stable spatial patterns by comparing against a large set of continuous fixed-site measurements from a sampling campaign in West Oakland, California. Custom-built, low-cost aerosol black carbon detectors (ABCDs) provided 100 days of continuous measurements at 97 near-road and 3 background fixed sites during summer 2017; two concurrently operated mobile laboratories collected over 300 h of in-motion measurements using a photoacoustic extinctiometer. The spatial coverage from mobile monitoring reveals patterns missed by the fixed-site network. Time-integrated measurements from mobile lab visits to fixed-site monitors reveal modest correlation (spatial R^2 = 0.51) with medians of full daytime fixed-site measurements. Aggregation of mobile monitoring data in space and time can mitigate high levels of uncertainty associated with measurements at precise locations or points in time. However, concentrations estimated by mobile monitoring show a loss of spatial fidelity at spatial aggregations greater than 100 m.

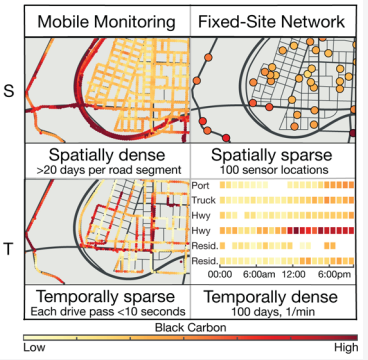

1. INTRODUCTION

Many urban areas exhibit highly localized variation in concentrations of primary air pollutants, including carbon monoxide (CO), nitric oxide (NO), and black carbon (BC) particles.[1−7] BC is a byproduct of incomplete combustion and a significant component of fine particulate matter. Important emission sources include diesel engines, industrial processes, and other carbonaceous fuel combustion.[8] Freshly emitted BC is primarily in the ultrafine size category (diameter <100 nm), while aged particles range in size up to ∼1.0 μm due to surface accumulation of secondary reaction products.[9,10] BC is a potent climate pollutant and is associated with numerous adverse health effects such as cardiovascular disease and lung cancer.[8,11,12] Within urban areas, steep spatial gradients of BC and other primary pollutants can result from spatial variation in traffic composition and density, localized emissions activity such as cooking or industrial operations, and topographical features such as mountains and street canyons.[2,4,5,7,13−18] Neighborhood- to street-scale variation can result in substantial differences between individual and population-level exposures, with important implications for epidemiology, air quality management, and environmental equity.[2,17,19,20] Direct measurement of fine-scale patterns can aid exposure evaluation by revealing spatial variation not captured by central-site monitoring and by detecting idiosyncratic features not included in predictive models.

Mobile monitoring directly measures spatial gradients and peaks in urban air pollution by using rapid-pass sampling to provide broad spatial coverage with a single set of instruments.[1,2,4−6,17,21−33] To provide representative estimates of long-term concentration patterns at high spatial resolution, a mobile monitoring study design must include (1) instruments capable of high-frequency measurements and (2) a driving schedule and pattern that captures representative conditions. The spatial resolution of mobile measurements depends directly on instrument response time and vehicle speed; for instance, 1 Hz measurements made at a driving speed of 10 m s^{-1} correspond to a 10 m spatial resolution. Most recent mobile monitoring campaigns that produced high spatial resolution BC maps (10−30 m) relied on instruments using a 1 Hz time resolution (see Table S1), most commonly the microAeth AE-51 (AethLabs, Incorporated) or the photo-

Received: March 6, 2020
Revised: June 7, 2020
Accepted: June 11, 2020
Published: June 11, 2020

acoustic extinctiometer (Droplet Measurement Technologies).[4,17,21,23,25,34,35] Instrument noise can be significant at high time resolution and is often increased by in-motion operation of equipment (e.g., owing to mechanical vibration).[5,36] Commonly applied noise reduction algorithms that rely on increasing the averaging periods may reduce the effective spatial resolution of mobile measurements.[37] Thus, efforts to improve measurement precision may come at the cost of detecting highly localized patterns.

Because a mobile lab can only measure at a single location at a time—providing temporally sparse coverage of any given site—a key challenge for mobile monitoring is to collect a temporally representative sample of concentrations for all microenvironments within a study area.[4−6,21,26,27,29,32,34,38] Although temporally unbalanced driving may be mitigated with background correction techniques, the uncertainty that arises from sampling error limits confidence in both the overall concentration estimates and the relative rankings of different microenvironments.[25,34,39] Monte Carlo data subsampling experiments have shown that meeting ±25% confidence bounds for BC requires anywhere from 10 to over 100 visits.[34,39] Microenvironments with higher temporal variability generally require more sampling.[17,21,34]

A key limitation of data experiments is that they are, by definition, based on a temporally sparse set of mobile monitoring samples that may not represent the full temporal variability at a point location. Continuous measurements at a fixed location provide a more rigorous basis for evaluating mobile monitoring within close proximity of the fixed site, but such comparisons are rare in the BC literature (see Table S1). One notable example from a campaign in Belgium found poor agreement among mobile measurements and simultaneous measurements made at nearby fixed sites (N = 3) but moderate to high agreement (R^2 between 0.53 and 0.96) among daily road segment and fixed-site averages.[21] Correlation between mobile monitoring and nearby fixed-site measurements depends on the degree of spatial heterogeneity in concentrations around the fixed point as well as instrument differences (e.g., instrument model or detection method). The temporal mismatch in measurements made during the same time period but at different time resolutions causes additional disagreement. An understanding of the relative importance of each factor can improve mobile monitoring study design and data interpretation but requires a larger data set.

The present analysis leverages data from an unusually dense network of low-cost BC sensors to compare mobile monitoring against continuous measurements at 97 near-road sites over 100 days. We use this rich data set to (1) to assess sources of error and bias that contribute to divergence between mobile and fixed-site air pollution measurements and (2) consider how uncertainty in the measurements from these two complementary techniques affects the interpretation of high-resolution air pollution maps. We also investigate the trade-off between greater sampling time versus increased spatial misalignment from the spatial aggregation of mobile measurements.

2. MATERIALS AND METHODS

2.1. Study Area and Sampling Design. We conducted mobile and fixed-site monitoring in West Oakland, California. West Oakland contains a mix of residential, commercial, and industrial land uses; two major highways; and several heavily trafficked routes servicing the Port of Oakland and other commercial and industrial sites.[40] West Oakland exhibited stable meteorology throughout the campaign, with 70% of wind measurements from the west or west-southwest and an average daytime windspeed between 3.5−5.2 m s^{-1}.[40] BC concentrations at the centrally located monitoring site operated by the Bay Area Air Quality Management District (BAAQMD) averaged 0.4 μg m^{-3} during the campaign, which is typical for summer conditions in this area. BC concentrations in this region exhibit strong seasonal variability, with higher ambient concentrations in winter (~1.4 μg m^{-3}) than summer.[18] Annual-average on-roadway daytime BC concentrations can exceed 2 μg m^{-3} BC along the most polluted road segments in the sampling domain.[17]

The fixed-site network ("100 × 100 BC Network") comprised 100 sites representative of residential, industrial, and high-traffic microenvironments at an average density of 6.7 sites per km^2.[40,41] One or more low-cost ABCD instruments were installed at each site, mounted at a height of 1.5 m on fences, porches, etc., at a median distance of 15 m from the nearest road. Of the 100 sites, 97 were located within 30 m of the road network covered by mobile monitoring, and 3 were at upwind background sites along the San Francisco Bay. Network operation during the 100-day period (May 19 through August 27, 2017) is detailed in Caubel et al.[40] Two mobile laboratories drove within West Oakland on 57 days during the same 100-day period, including 46 weekdays and 12 weekend days, for a total of 304 sampling hours. Mobile monitoring was limited to daytime hours, with most coverage during of 8 am−6 pm (Figure S1). Mobile laboratories repeatedly sampled air quality in a "blackout" pattern covering all roads within subsections of West Oakland. Mobile monitoring data from Summer 2017 are presented for the first time here, expanding on a previous data set collected from May 28, 2015 to May 19, 2017, as described in Apte et al.[17] and Messier et al.[42] Subsections of the domain were driven on a rotating schedule to minimize temporal sampling bias.

The sampling design provided two ways in which the mobile lab could be located near to the fixed-site measurements. First, during normal on-road driving for the mobile lab, the mobile lab passed in close proximity to the fixed-site instruments. Over the course of the campaign, this type of brief drive-by colocation occurred dozens of times for each monitor (Tables 1 and 2). In total, 88 h of data were collected for which the

Table 1. Mobile Monitoring Sample Size for Different Buffer Lengths

	30 m buffer	95 m buffer
Visits Per Site		
total sites included	90	97
10th percentile	14	27
median	23	73
90th percentile	69	142
Duration of Individual Visits		
10th percentile	2 s	6 s
median	4 s	17 s
90th percentile	10 s	36 s
Total Sampling Time Per Site		
10th percentile	71 s (1.2 min)	576 s (9.6 min)
median	200 s (3.3 min)	1761 s (29.3 min)
90th percentile	667 s (11.1 min)	3472 s (57.9 min)
cumulative duration across all sites	8.6 h	55.6 h

https://dx.doi.org/10.1021/acs.est.0c01409
Environ. Sci. Technol. 2020, 54, 7848−7857

mobile lab was within 150 m of a fixed-site instrument. Second, the mobile lab was parked periodically near two fixed-sites with ABCD instruments and commercial BC instruments (Aethalometer model AE33, Magee Scientific). These colocations provide an in situ comparison among the three detection methods. In total, 3.7 h of data were collected during this type of intentional stationary colocation.

2.2. Measurement Methods. *2.2.1. Fixed-Site Instruments.* The fixed-site network was composed of 128 custom-built low-cost Aerosol Black Carbon Detectors (ABCD), described in detail by Caubel et al.[41] In brief, the ABCD uses a filter-based light absorption technique to relate light attenuation on a filter to changes in BC mass loading, similar to an aethalometer.[43] Attenuation measurements are corrected for temperature, relative humidity, and loading artifacts before making a final determination of mass concentration. Post-correction data at a 1-h averaging time show a fleet average precision of 9.2% and accuracy of 24.6% evaluated relative to a commercial BC instrument (Aethalometer model AE33, Magee Scientific). As configured here, the ABCD measured at a maximum time resolution of 0.5 Hz, with averaging times of 2 s to 1 min used in our analysis.

2.2.2. Mobile Monitoring. Two Google Street View (GSV) vehicles were equipped with the mobile instrumentation platform described by Apte et al.[17] Black carbon was measured at 1 Hz time resolution using a photoacoustic extinctiometer (PAX; Droplet Measurement Technologies, Boulder, CO). The PAX performs a 70 s automatic zero calibration procedure every 10 min during operation to maintain instrument performance. To compensate for additional instrumental drift, measurements from both PAX instruments were harmonized using a third, recently calibrated PAX operated at the mobile lab parking facility. We evaluate: agreement among instruments using R^2 from least-squares regression; relative precision based on mean absolute error (MAE), root-mean-square error (RMSE), and normalized root-mean-square error (NRMSE); and bias based on mean bias error (MBE) and fitted linear equations. Metrics are defined in Section S1.1 of the Supporting Information. Postadjustment PAX-to-PAX comparison shows high correlation and small relative bias (R^2 = 0.97, MAE = 0.08 μg m^{-3}, NRMSE = 15%, MBE = −0.02 μg m^{-3}; see Table S2).

During in-vehicle operation, PAX measurements show instrument noise at 1 Hz that can exceed observed BC concentrations, making the mitigation of noise central to this analysis. We quantify noise as the standard deviation around zero (σ_0) of measurements made with filtered air. On the basis of readings during self-calibration events and operation of the mobile lab with a filtered inlet, PAX instrument noise at 1 Hz ranges from 0.20 μg m^{-3} at vehicle speeds <5 m s^{-1} to 0.59 μg m^{-3} for average in-motion operation. Because noise is known to decrease in proportion to time integration period n, we derive an empirical formula for $\sigma_0(n)$ using in-operation noise measurements at 1 and 0.1 Hz and estimates of σ_0 at averaging windows from 1 to 60 min from garage colocation data using the Grubbs 3-instrument technique (Table 2).[44] We derived the following power-law relationship for instrumental noise based on a linear fit of log-transformed σ_0 and n distributions, shown in Figure S2

$$\sigma_0 = 0.55 \times n^{-0.27} \quad (1)$$

where n = time integration period (seconds) and σ_0 = standard deviation around 0 (μg m^{-3}).

Table 2. Instrument Noise σ_0 at Different Averaging Times (μg m^{-3})

averaging time (min)	ABCD	PAX
0.017 (1 s)		0.59
0.17 (10 s)		0.31
1	0.14	0.16
5	0.05	0.12
20	0.03	0.08
60	0.02	0.05
1440 (24 h)	0.001	0.02

This result is in line with observations that in-operation noise reduces quickly with increasing integration time scales. We reference two metrics derived from $\sigma_0(n)$: the effective limit of detection (LOD; eq 2) and instrument precision expressed as the bounding value for 95% confidence in the PAX measurement (eq 3).

$$\mathrm{LOD}(n) = 3 \times \sigma_0(n) \quad (2)$$

$$\mathrm{Precision}(n) = \pm 2 \times \sigma_0(n) \quad (3)$$

This corresponds to a precision of 0.16 μg m^{-3} and an effective LOD of 0.24 μg m^{-3} for 20 min of cumulative sampling time, a typical time-integration period from the set of repeated mobile visits to a fixed site during this campaign.

PAX data were processed to remove measurements taken during periodic instrument self-calibration operations (10% of data) and any measurement period with a 2 min moving average less than zero, reflecting atypical instrument drift between self-calibration operations (0.6% of the data). Sampling the vehicle's own exhaust plume, evidenced by a rapid increase in concentrations of multiple pollutants, was only observed to occur during certain wind conditions while the vehicle was idling. All idling data (vehicle speed = 0) were excluded from this analysis.

2.2.3. Evaluation of Instrumental Differences. Three ABCD instruments were colocated with both PAX instruments for 183 h in a semienclosed garage along the Embarcadero in San Francisco where routine mobile lab maintenance was performed. Major nearby BC sources include diesel vehicles and marine vessels. Concentrations at a 1 min averaging time ranged from <0.1−8 μg m^{-3}. The set of instrument comparison metrics described above are provided in Tables S3 and S4 for two sets of averaging periods: 1 min averages for both instruments, corresponding to the time integration period for a low level of mobile sampling (e.g., six 10-s visits), and 20 min averages, corresponding to a high sampling rate (e.g., 120 10-s visits).

Pairwise regressions between ABCD and PAX operating in the garage show correlations that are high for 20 min averaging (R^2 = 0.85 to 0.91) and slightly (~8%) lower and more variable among instruments for 1 min averaging (R^2 = 0.64 to 0.86). PAX-to-ABCD precision at 20 min, MAE = 0.16 μg m^{-3} and RMSE = 0.26 μg m^{-3}, is approximately 20% of typical hot spot or highway concentrations but of comparable magnitude to summertime concentrations of 0.3 μg m^{-3} in relatively cleaner neighborhoods in West Oakland. MAE and RMSE are 25% and 30% higher, respectively, with 1 min averages than with 20 min averages. We observe low relative bias among instruments with fitted linear equations; MBE showing a tendency of PAX instruments to read 10 to 15% lower than the compared ABCD devices (MBE = 0.03 μg m^{-3}). Because the

https://dx.doi.org/10.1021/acs.est.0c01409
Environ. Sci. Technol. 2020, 54, 7848−7857

bias observed in these three ABCD instruments may not be representative of the total ABCD fleet, we did not apply adjustment factors to PAX instruments based on these comparisons; in situ MBE across the entire ABCD fleet was moderate (~0.1 μg m^{-3}; see Figure 4), but a sensitivity analysis indicated that bias adjustment had a marginal effect on the MAE of in situ comparisons and no effect on correlation coefficients. In comparing measurements from two different detection methods, we inherently assume that both methods will respond equivalently to BC particles of varying source or age under all relevant environmental conditions. We believe this assumption is justified, as (1) the ABCD measurements include adjustments for humidity effects and a filter loading artifact, (2) the garage colocation measurements show a strong linear correlation between the two analyzers, and (3) previous evaluations validate the relative instrumental response of photoacoustic and filter-based BC measurements under laboratory and field conditions.[45,46]

2.3. Spatial Patterns of Black Carbon in West Oakland. To provide context for the core quantitative mobile vs fixed-site comparison, we provide here a qualitative comparison of West Oakland BC spatial patterns revealed by both methodologies. For map-based visualization of mobile monitoring, we join mobile lab global positioning system (GPS) coordinates to the nearest 30 m road segment, record the mean of each drive pass, and calculate for each road segment the median value of all drive-pass means, as described in detail by Messier et al.[42] We create two additional maps with data processed with a 10 and 20 s moving average, corresponding to an approximate spatial smoothing of 90 and 190 m (average nonhighway vehicle speed of 9.3 m s^{-1}). We calculate the effective LOD for each road segment and averaging period as described in Section S1.2. Effective LOD varies by road segment and decreases at longer averaging periods (see distributions in Figure S3). For the 1 Hz mobile data, concentrations at approximately half of the road segments are indistinguishable from 0 based on effective LOD (Figure S4a). Shifting from 1 to 20 s moving average (Figure S4c), the median LOD decreases by 30%, producing a more spatially complete map with some loss of resolution of highly localized spatial heterogeneity.

The mobile monitoring map from 20 s moving average data shows the same general spatial patterns as fixed-site daytime medians (Figure 1). Measurements at the road segment level also reveal localized patterns not detected by the fixed-site network, with examples marked **a**–**d** (street-level images of these areas are provided in Figure S5). Mobile monitoring provides measurements on highways where placement of fixed-site monitors may be infeasible. Mobile coverage near **a** shows the increase in concentration on elevated sections of Interstates 880 and 580 compared to the adjacent road network, as well as concentration reduction with distance from highways. Industrial activity near **b**, including a cement plant and metals recycling facility,[17] is reflected in elevated concentrations at nearby fixed sites, while mobile monitoring also captures several additional highly localized "hot spots." Road-segment medians also show hot spots corresponding to specific routes such as the intersection segment at **c**, which acts as a funnel for truck traffic to the Port of Oakland. Concentration peaks along roads like the designated truck route around the Port of Oakland south of **d** may reflect persistent small-scale differences in patterns of traffic congestion. Thus, mobile monitoring adds local context to the more precise, time-resolved measurements at fixed sites.

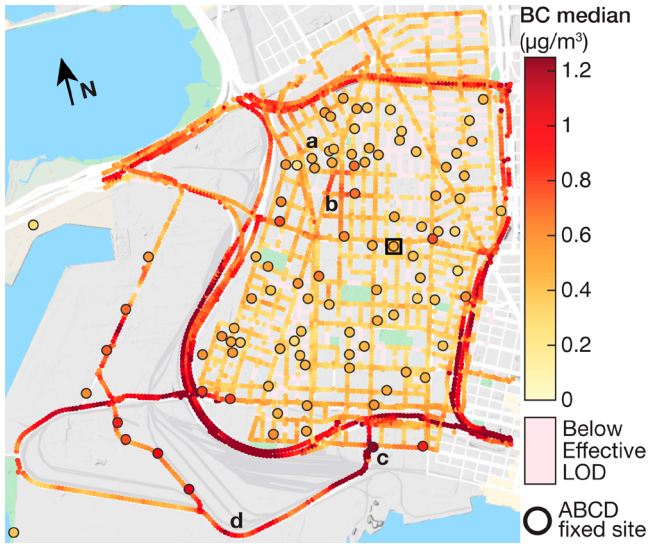

Figure 1. Median black carbon (BC) concentration measured during daytime hours (9 am–5 pm) throughout the 100-day campaign. Circles represent median ABCD measurements at fixed sites and on-road coloration shows smoothed mobile monitoring data (20 s moving average), represented as the median of drive-pass means calculated for 30 m road segments. The square icon in center of map represents the single regulatory fixed monitoring site in the domain. Labels a–d correspond to specific locations described in detail in text. Map data: © 2020 Google.

As one illustration of the potential value of mobile monitoring, 78% of mobile monitoring data was collected at a distance greater than 100 m from any fixed site (see Figure 2). Consistent with Figure 1, the upper tail (top 5%) of the distribution (Figure 2a) shows highway road segment medians, many of which exceed 1.25 μg m^{-3}. Fixed-site hot spots (>0.80 μg m^{-3}) appear as isolated peaks of 1–2 monitors in Figure 2b, matched in Figure 2a by a small share of near-site mobile monitoring data and a large share of additional mobile monitoring data collected in interstitial areas. The overall median among fixed sites (0.48 μg m^{-3}) closely matches that of nonhighway road segments (0.44 μg m^{-3}). These similar medians suggest that nonhighway data collected on-road are broadly representative of near-road concentrations despite closer proximity to tailpipe emissions.

2.4. Mobile and Fixed-site Comparisons. Our core quantitative analysis considers how successfully the temporally sparse set of mobile measurements can determine time-integrated concentrations at specific locations, given the uncertainty from sampling error and instrument noise. We also investigate the trade-off between spatial resolution and the temporal density of mobile data. To process mobile data for this comparison, mobile lab GPS coordinates are used to calculate the instantaneous distance of the mobile lab from each fixed site, without any "snapping" of observations to the road network geometry. The series of 1 Hz mobile measurements made within a given buffer length from a fixed site compose a single unique sample ("visit") for which we calculate the mean of mobile measurements and mean of contemporaneous fixed-site measurements. To reduce temporal sampling bias, we only include visits made during daytime hours (9 am –5 pm), which were most evenly sampled. At a

https://dx.doi.org/10.1021/acs.est.0c01409
Environ. Sci. Technol. 2020, 54, 7848–7857

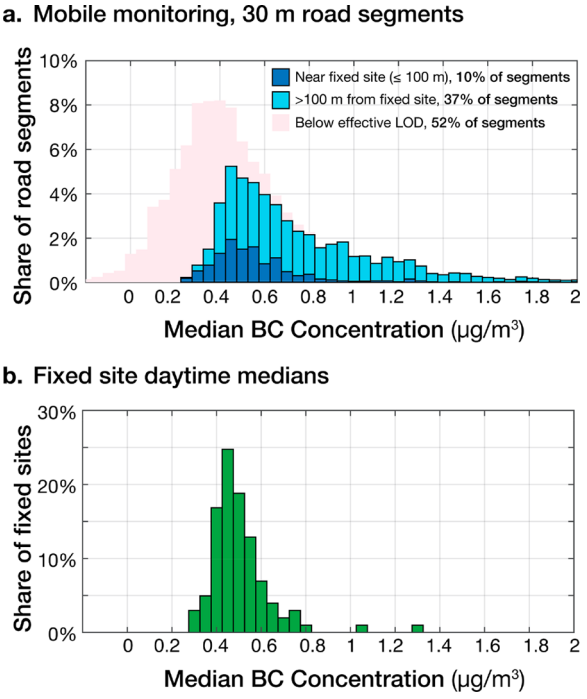

Figure 2. Histograms of median mobile monitoring concentrations by road segment within the study domain (a) and median daytime fixed-site concentrations (b). Road segment medians are calculated from 1 Hz data; values correspond to Figure S4a. Mobile monitoring is divided into data collected within 100 m of a fixed site, which constitutes 22% of spatial coverage over the effective LOD, and data collected beyond 100 m from a fixed site, constituting 78% of spatial coverage.

buffer of 95 m, daytime mobile monitoring resulted in a 10th–90th percentile range of 27 to 142 visits and 10 to 58 min of total in-motion sampling time at each site (Table 2). The median of visit means at each site is used as a representative metric of the time-integrated concentration over the whole campaign. Visit-based concentration estimates are compared with the 100-day median of ABCD measurements made during daytime hours at each site.

We use the set of metrics described in Section S1.1 to evaluate the core comparison (**i**) of mobile monitoring and 100-day fixed-site daytime medians. Sources of disagreement in this comparison fall into the four categories listed in Table 3: detection method differences, instrument noise, sampling error, and spatial misalignment. We include two supplementary comparisons to the effects of some of these sources of disagreement. The contemporaneous subsample comparison (**ii**) considers error and bias between mobile monitoring and the medians of ABCD measurements made concurrently with mobile lab visits at each site (fixed-site temporal subsample). Because sampling periods align very closely, sampling error has a marginal effect on the comparison, highlighting the effects of spatial misalignment and detection method differences. However, the reduced cumulative sampling time for the ABCDs increases the effect of ABCD instrument noise. Here, we use the 1 min resolution ABCD measurements most closely matched in time to each drive pass, which introduces a minor degree of temporal mismatch sampling error relative to using ABCD data at their native 0.5 Hz resolution but with the benefit of a substantial reduction in instrument noise (see Figures S6–S8).

Table 3. Sources of Disagreement for Each Comparison Category

	detection method	instrument noise[1]	sampling error	spatial misalignment
i. Core Result				
Mobile monitoring during visits vs all daytime ABCD measurements	X	X	X	X
ii. Contemporaneous Subsample				
Mobile monitoring during visits vs ABCD measurements during visits	X	X		X
iii. Temporal Representativeness				
ABCD measurements during visits vs all daytime ABCD measurements		X	X	

[1]The effect of instrument error is different for each comparison, as short-duration averaged ABCD, long-duration averaged ABCD, and short-duration averaged PAX measurements each exhibit different instrument errors (see Table 1).

The temporal representativeness comparison (**iii**) uses only fixed-site data to evaluate whether the conditions during mobile sampling, represented by the temporal subsample of fixed-site data used for comparison **ii**, vary significantly from overall daytime conditions, represented by the 100-day fixed-site daytime medians. Thus, we compare the overall median of summer daytime concentrations to a median from 0.007% of all measurements. This comparison is only affected by sampling error and ABCD instrument noise, removing the effects of detection-method differences and spatial misalignment.

We investigate the sensitivity of our comparison metrics to varying levels of spatial aggregation by varying the buffer length used to define a visit between 30 and 150 m. Because 11 fixed sites were located more than 25 m from the nearest road, we did not consider buffer lengths less than 30 m in this sensitivity analysis. The number of visits, visit length, and total sampling time per site at 30 and 95 m are shown in Table 1: at 95 m, median visit count is more than doubled and total sampling time increases by a factor of 7. While sampling error and instrument precision benefit from these increases, the increase in spatial misalignment between mobile and fixed-site measurements may reduce the ability of mobile monitoring to distinguish localized concentration patterns.

Finally, we consider two spatiotemporal comparisons of the mobile and fixed-site data. First, we compare spatial patterns and correlation results for weekday mobile and fixed-site medians and weekend medians. Second, we analyze agreement between individual contemporaneous mobile and fixed-site measurements during brief in-motion visits and short stationary colocation events.

3. RESULTS AND DISCUSSION

3.1. Comparison of Site Medians. At a moderately localized spatial scale (buffer distance of up to 95 m), mobile monitoring reproduces fixed-site daytime median concentrations with a mean average error within the bounds of instrument precision limits (MAE = 0.11 μg m^{-3}, 95% precision ±0.15 μg m^{-3}). The majority of points are clustered within the range of 0.4 to 0.7 μg m^{-3} (Figure 3a), typical of residential and commercial area concentrations. Approximately 20% of points occur at concentrations greater than 0.7 μg m^{-3},

https://dx.doi.org/10.1021/acs.est.0c01409
Environ. Sci. Technol. 2020, 54, 7848–7857

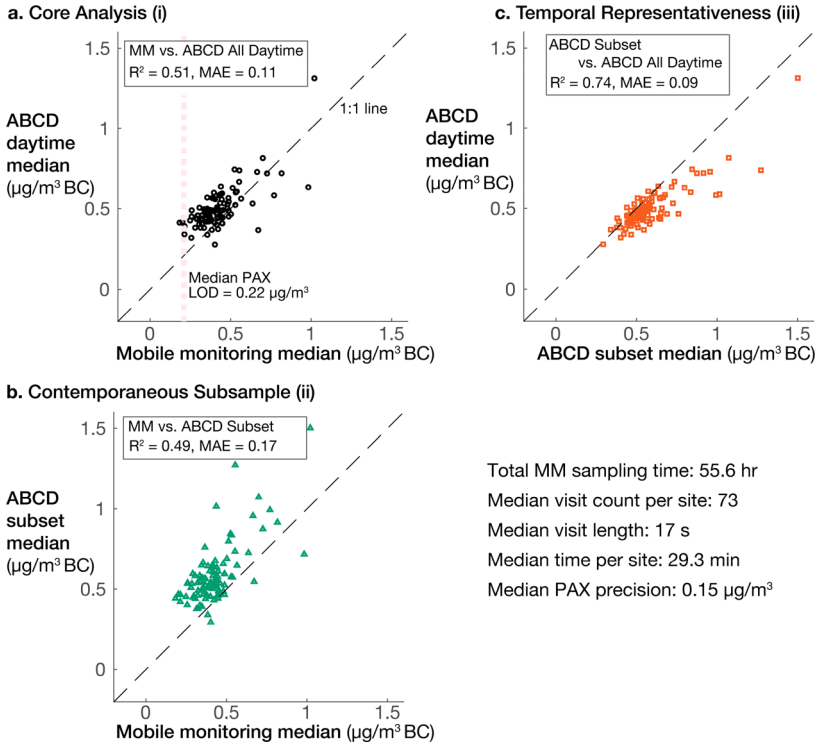

Figure 3. Using a fixed-site radius of 95 m, pairwise correlation between median BC concentrations measured by three distinct data sets: mobile monitoring visits (MM), ABCD measurements made during all daytime hours throughout the campaign (ABCD All Daytime), and the temporal subset of ABCD measurements made during mobile monitoring visits (ABCD subset). Figure 3a shows results for the core analysis with the median effective limit of detection (LOD) for PAX mobile measurements indicated by the vertical dotted line. Given nearly continuous monitoring, the LOD for ABCD daytime medians is $\ll$0.01 μg m^{-3}. Figure 3b shows the first supplemental comparison: mobile monitoring medians compared with the medians of ABCD measurements made concurrently with mobile lab visits to each site (contemporaneous subsample). The mobile monitoring LOD is the same as in 3a, and the LOD for ABCD subset medians is approximately 0.05 μg m^{-3}. Figure 3c shows the second supplemental comparison: the subsample of ABCD medians calculated during mobile lab visits compared with the medians from the complete set of daytime measurements.

indicative of high traffic or industrial activity (cf. Figure 1). Fixed-site and mobile in-motion medians are correlated (R^2 = 0.51), despite method differences and temporal sparsity. The contemporaneous subsample comparison **ii**, intended to highlight method differences, instead shows that the higher level of ABCD instrument noise at short averaging periods results in slightly lower correlation, despite a more temporally matched sampling of the fixed-site measurements. The fixed-site temporal sparsity test **iii** shows high correlation and moderate error levels between the fixed-site temporal subset and overall daytime medians (R^2 = 0.74, MAE = 0.09 μg m^{-3}), suggesting a moderate degree of sampling error coupled with the effect of ABCD noise. It is worth noting that this temporally sparse subsample of ABCD measurements, representing approximately 70 random point-in-time measurements per site, successfully approximates the central tendency of continuous fixed-site measurements within moderate error bounds. Thus, a key inference is that even an extremely temporally sparse set of temporally random fixed-site measurements can reproduce the long-term average of continuous measurements.

For a highly localized comparison (buffer distance of up to 30 m), mobile monitoring shows poorer performance at reproducing fixed-site medians (MAE = 0.19 μg m^{-3}, R^2 = 0.36; see Figure S9), owing principally to increased instrumental noise at shorter integrating time scales. This change in buffer length (95m down to 30m) decreases the area of inclusion around each fixed site by an order of magnitude, and the average vehicle-to-site distance decreases from 66 to 21 m (Figure S10), decreasing spatial misalignment at the cost of dramatically decreasing sample size: a 6× decrease in median time per site and a 3× reduction in visits per site (Table 2). The reduced time integration period increases median effective LOD by 3×, to 0.39 μg m^{-3}, and medians at 60% of sites fell below the effective LOD. Variance among mobile monitoring medians is greatly increased for a smaller buffer size (Figure S9), in line with a substantial reduction in effective PAX instrument precision. The contemporaneous subsample comparison **ii** shows similarly weakened correlation, but the temporal sparsity comparison **iii** shows only a small reduction in correlation and increase in error (R^2 = 0.68, MAE = 0.11 μg m^{-3}). A limited examination of correlation between fixed-site and mobile in-motion medians by land use category (e.g., port, truck route, residential) suggests that (1) in areas with consistently high concentrations such as along truck routes, correlation in the core comparison tends to be higher and normalized error tends to be lower compared to low-concentration residential areas, and (2) temporal representativeness is higher for truck routes than residential areas (see S2.1). We tentatively interpret these results as an emergent property of signal-to-noise ratio: all else being equal, higher signal-to-noise (e.g., along truck routes) improves measurement fidelity.

The dependence of R^2, MAE, and MBE on spatial aggregation scale (and on the corresponding increase in visit count and instrument precision) is shown further in Figure 4.

https://dx.doi.org/10.1021/acs.est.0c01409
Environ. Sci. Technol. 2020, 54, 7848−7857

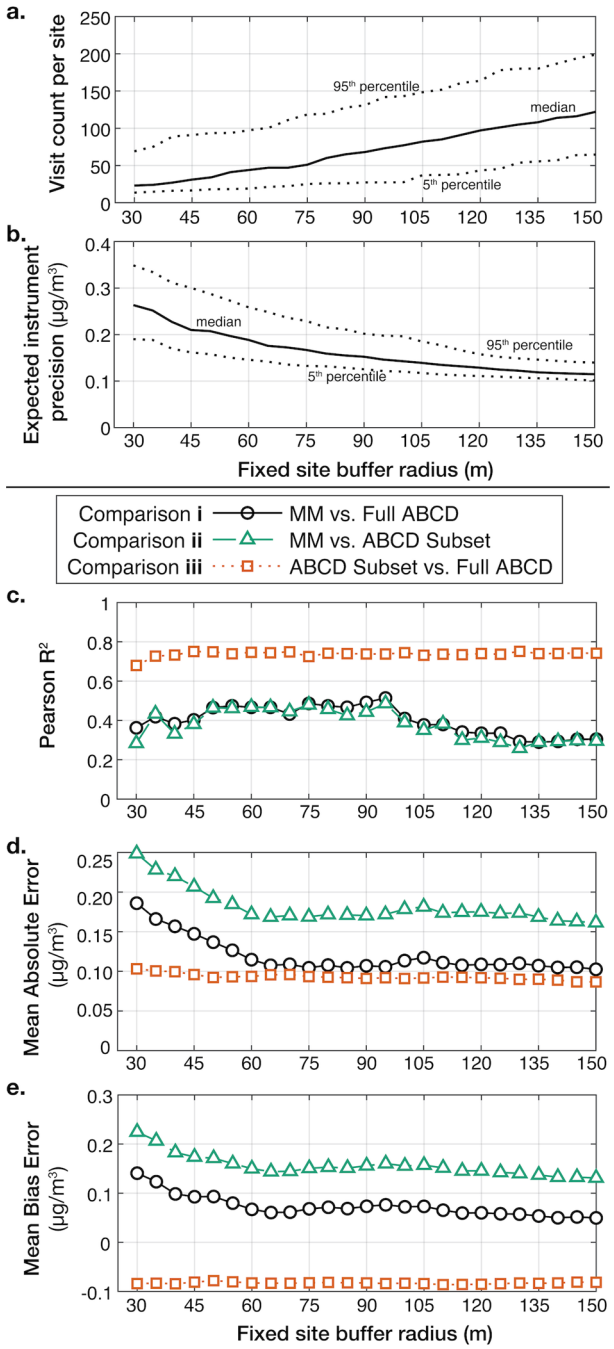

Figure 4. Change in sample size, Pearson's R^2, mean absolute error (MAE), and mean bias error (MBE) with increasing fixed-site buffer length.

The trend in the core comparison correlation (Figure 4c, black line) suggests that the trade-off in correlation strength between sample size and spatial misalignment shifts at a buffer length of approximately 95 m. Mean absolute error (Figure 4d, black line) reaches a minimum at a length of 65 m—in line with increased mobile monitoring precision (Figure 4b)—and shows no further trend with buffer length. The MAE for comparison **ii** (Figure 4d, green line) shows a consistent margin of 0.05 $\mu g\ m^{-3}$ above the core comparison, reflecting the increase of ABCD instrument noise when incorporating a small number of visits rather than the campaign average. That instrument noise is also reflected in the comparison **ii** correlation trend (Figure 4c, green line), which does not exceed correlation for the core comparison but does increase with buffer distance up to 95 m. The close pairing of the comparison **i** and **ii** correlation trends suggests that mitigating instrument noise drives the improvement in correlation with increasing spatial aggregation, further evidenced by the relatively constant correlation and error trends of the fixed-site temporal representativeness comparison (**iii**) (Figure 4c,d, orange line).

Mean bias error for both comparison **i** and **ii** stabilizes at 65 m, and it remains approximately constant for comparison **iii**. The stable MBE values indicate that sampling occurred during moderately more polluted conditions (comparison **iii** MBE = $-0.08\ \mu g\ m^{-3}$), but mobile measurements are biased low in comparison with fixed sites (comparison **ii** MBE = $0.15\ \mu g\ m^{-3}$), resulting in a lower MBE for the core comparison. Temporal sampling bias resolved by site is consistent with these patterns (Figure S11). Restricting mobile sampling to daytime hours increases bias compared to 24 h medians, which are typically 15% lower (see S2.4). Periods of elevated background concentration due to long-range transport events could potentially affect the strength of correlation and temporal bias, but we found our results were not sensitive to the exclusion of days with elevated background concentration (see S2.3).

3.2. Spatiotemporal Comparison. Weekday and weekend conditions in West Oakland vary significantly in both the range of concentrations and the degree of spatial heterogeneity (see maps in Figure S12). Several spatial patterns in both fixed-site and mobile monitoring maps reflect weekday emissions activity, including port-related traffic and industrial activity in the northwest quadrant of the domain (Figure S11). Relative to weekends, weekdays exhibit higher correlation for the core comparison (R^2: 0.45 vs 0.03), but lower MAE values (0.13 vs 0.18; units: $\mu g\ m^{-3}$; Table S5), partially reflecting differences in sample size. The spatial coverage of mobile monitoring data shows the distribution and intensity of weekday emissions activities within the domain, complementing detailed information about diurnal concentration cycles measured at fixed sites.[36]

While the weekday-weekend comparison shows that mobile monitoring can reveal changes in spatial patterns for coarse temporal divisions (e.g., weekday vs weekend), the high degree of instrument noise relative to ambient concentrations in this study inhibits the ability of mobile monitoring to provide reliable measurements at full spatiotemporal resolution (i.e., point-in-time estimates for a specific location from a single drive pass). Aggregated across all sites, contemporaneous mobile and fixed-site measurements during in-motion visits show no correlation, regardless of buffer length (Table S6). Correlation at individual sites is also poor, both when comparing mobile monitoring to ABCD instruments and AE33 reference instruments (see S2.4; Tables S7–S12, Figures S15–S20). However, a supplementary set of experiments where cars repeatedly parked for several minutes next to fixed monitoring sites suggests that correlation in contemporaneous measurements improves dramatically when site visits are lengthened from ~20 s in-motion (R^2 = 0.05) to ~7 min parked within 80 m of the site (R^2 = 0.65). The difference in performance between in-motion and short-term stationary colocations suggests that in cases where spatially distributed, real-time estimates of concentrations are desired, instrument

https://dx.doi.org/10.1021/acs.est.0c01409
Environ. Sci. Technol. 2020, 54, 7848−7857

noise may be overcome by extending sampling time at locations of interest.

3.3. Recommendations for Future Research. Through this comparison of measurement paradigms, we find that full-coverage mobile monitoring can effectively fill in the gaps in spatial patterns shown by a fixed-site network, and that spatial aggregation can mitigate instrument noise through an increase in per-spatial-unit sampling time. The need to reduce effective BC instrument noise is of increased importance in the comparatively clean conditions of this summer campaign, where instrument noise and background concentrations were of similar magnitude. Under such conditions, this analysis showed that mobile monitoring provides reasonable spatial fidelity at a buffer size of 95 m (or spatial resolution of ∼0.03 km^2). Resolving spatial heterogeneity on a substantially finer scale, (e.g., 10−20 m), which is often the goal of mobile monitoring campaigns,[4,21,23,25,35] may be more readily achieved in environments where instrument noise is low relative to ambient conditions and the magnitude of spatial gradients. The resolution of more subtle heterogeneity may require an increase in both the number of visits made and the duration of each visit (i.e., by slowing or temporarily stopping the vehicle). Results of this study can inform the design of future campaigns.

Following the findings that spatial resolution is affected by instrument noise and averaging time, future mobile monitoring analyses should explicitly consider the appropriate level of spatial aggregation. Future work could routinize this element of study design through a parametrized model that considers the magnitude of different sources of error. Because spatial aggregation may differ among microenvironments, such modeling may include further analysis of results divided by land-use type using carefully balanced subsamples. Study goals may also influence the desired level of spatial aggregation. For example, higher spatial resolution may be used to address research questions that can accommodate wider uncertainty bounds, such as identifying hot spots that exceed regional background concentrations by an order of magnitude.

The techniques used here for comparing mobile and fixed-site comparisons could usefully be extended through further data experiments. Since these findings suggest that instrument noise and not sample size is the prevailing source of error, this data set could support the use of randomized or controlled subsamples of fixed-site and mobile data to test the effectiveness of different mobile monitoring deployment strategies. This may include the direction of more sampling during certain time periods or in certain areas. A limit to such a study is the limited window of sampling; sampling error may account for a greater share of uncertainty in studies that distribute sampling over longer periods that are affected by greater seasonal variability in measured concentrations.

This analysis also highlights the strength of a fixed-site network in providing distributed real-time measurements, acting as a valuable complement to mobile monitoring efforts. Under the conditions of this campaign, mobile monitoring showed poor performance in providing temporally resolved measurements at fixed sites. For such purposes, mobile laboratories may be more effectively employed in conducting short-term stationary measurements.

The combination of mobile and fixed measurements into a single sampling campaign provides highly detailed information on both spatial and temporal trends in air quality within individual neighborhoods. Following this effort in the evaluation of methods to successfully compare and cross-validate these approaches, future work could usefully examine methods for fusing mobile and fixed-site measurements to estimate the spatiotemporal variability of air pollution across a measurement domain.

■ ASSOCIATED CONTENT

Supporting Information

The Supporting Information is available free of charge at https://pubs.acs.org/doi/10.1021/acs.est.0c01409.

Comparison metrics, calculation of effective LOD, analysis by land use category, instrument and temporal sampling bias ratios, sensitivity to long-range transport events, in-motion co-location vs short-term stationary co-location, figures, tables, and references (PDF)

■ AUTHOR INFORMATION

Corresponding Author

Joshua S. Apte − *Department of Civil, Architectural and Environmental Engineering, University of Texas at Austin, Austin, Texas 78712, United States; Department of Civil and Environmental Engineering and School of Public Health, University of California, Berkeley, Berkeley, California 94720, United States;* orcid.org/0000-0002-2796-3478; Email: apte@berkeley.edu

Authors

Sarah E. Chambliss − *Department of Civil, Architectural and Environmental Engineering, University of Texas at Austin, Austin, Texas 78712, United States;* orcid.org/0000-0002-6170-1789

Chelsea V. Preble − *Department of Civil and Environmental Engineering, University of California, Berkeley, Berkeley, California 94720, United States; Energy Technologies Area, Lawrence Berkeley National Laboratory, Berkeley, California 94720, United States;* orcid.org/0000-0002-6489-5718

Julien J. Caubel − *Energy Technologies Area, Lawrence Berkeley National Laboratory, Berkeley, California 94720, United States; Department of Mechanical Engineering, University of California, Berkeley, Berkeley, California 94720, United States*

Troy Cados − *Department of Civil and Environmental Engineering, University of California, Berkeley, Berkeley, California 94720, United States; Energy Technologies Area, Lawrence Berkeley National Laboratory, Berkeley, California 94720, United States*

Kyle P. Messier − *Department of Civil, Architectural and Environmental Engineering, University of Texas at Austin, Austin, Texas 78712, United States; Environmental Defense Fund, Austin, Texas 78701, United States;* orcid.org/0000-0001-9508-9623

Ramón A. Alvarez − *Environmental Defense Fund, Austin, Texas 78701, United States*

Brian LaFranchi − *Aclima, Inc., San Francisco, California 94111, United States*

Melissa Lunden − *Aclima, Inc., San Francisco, California 94111, United States*

Julian D. Marshall − *Department of Civil and Environmental Engineering, University of Washington, Seattle, Washington 98195, United States;* orcid.org/0000-0003-4087-1209

Adam A. Szpiro − *Department of Biostatistics, University of Washington, Seattle, Washington 98195, United States*

https://dx.doi.org/10.1021/acs.est.0c01409
Environ. Sci. Technol. 2020, 54, 7848−7857

Thomas W. Kirchstetter − *Department of Civil and Environmental Engineering, University of California, Berkeley, Berkeley, California 94720, United States; Energy Technologies Area, Lawrence Berkeley National Laboratory, Berkeley, California 94720, United States*

Complete contact information is available at: https://pubs.acs.org/10.1021/acs.est.0c01409

Notes

The authors declare no competing financial interest.

■ ACKNOWLEDGMENTS

We are grateful for contributions from D. Miller, K. Tuxen-Bettman, A. Raman, R. Moore, D. Herzl, and M. Chu Baird. This work was supported by the Environmental Defense Fund and the Health Effects Institute (HEI), an organization jointly funded by the US EPA (Assistance Award No. R-82811201) and certain motor vehicle and engine manufacturers. This publication was also developed as part of the Center for Air, Climate, and Energy Solutions (CACES), which was supported under Assistance Agreement No. R835873 awarded by the U.S. Environmental Protection Agency. It has not been formally reviewed by EPA. The views expressed in this document are solely those of authors and do not necessarily reflect the views of HEI, or its sponsors, nor do they necessarily reflect the views and policies of the EPA or motor vehicle and engine manufacturers. EPA does not endorse any products or commercial services mentioned in this publication.

■ REFERENCES

(1) Massoli, P.; Fortner, E. C.; Canagaratna, M. R.; Williams, L. R.; Zhang, Q.; Sun, Y.; Schwab, J. J.; Trimborn, A.; Onasch, T. B.; Demerjian, K. L.; Kolb, C. E.; Worsnop, D.; Jayne, J. T. Pollution Gradients and Chemical Characterization of Particulate Matter from Vehicular Traffic near Major Roadways: Results from the 2009 Queens College Air Quality Study in NYC. *Aerosol Sci. Technol.* **2012**, *46* (11), 1201−1218.

(2) Wu, H.; Reis, S.; Lin, C.; Beverland, I. J.; Heal, M. R. Identifying Drivers for the Intra-Urban Spatial Variability of Airborne Particulate Matter Components and Their Interrelationships. *Atmos. Environ.* **2015**, *112*, 306−316.

(3) Venkatachari, P.; Zhou, L.; Hopke, P. K.; Felton, D.; Rattigan, O. V.; Schwab, J. J.; Demerjian, K. L. Spatial and Temporal Variability of Black Carbon in New York City. *J. Geophys. Res. Atmospheres* **2006**, *111* (D10), 6314 DOI: 10.1029/2005JD006314.

(4) Levy, I.; Mihele, C.; Lu, G.; Narayan, J.; Hilker, N.; Brook, J. R. Elucidating Multipollutant Exposure across a Complex Metropolitan Area by Systematic Deployment of a Mobile Laboratory. *Atmos. Chem. Phys.* **2014**, *14* (14), 7173−7193.

(5) Padró-Martínez, L. T.; Patton, A. P.; Trull, J. B.; Zamore, W.; Brugge, D.; Durant, J. L. Mobile Monitoring of Particle Number Concentration and Other Traffic-Related Air Pollutants in a Near-Highway Neighborhood Over the Course of a Year. *Atmos. Environ.* **2012**, *61*, 253−264.

(6) Sullivan, R. C.; Pryor, S. C. Quantifying Spatiotemporal Variability of Fine Particles in an Urban Environment Using Combined Fixed and Mobile Measurements. *Atmos. Environ.* **2014**, *89*, 664−671.

(7) Gu, P.; Li, H. Z.; Ye, Q.; Robinson, E. S.; Apte, J. S.; Robinson, A. L.; Presto, A. A. Intracity Variability of Particulate Matter Exposure Is Driven by Carbonaceous Sources and Correlated with Land-Use Variables. *Environ. Sci. Technol.* **2018**, *52* (20), 11545−11554.

(8) Bond, T. C.; Doherty, S. J.; Fahey, D. W.; Forster, P. M.; Berntsen, T.; DeAngelo, B. J.; Flanner, M. G.; Ghan, S.; Kärcher, B.; Koch, D.; Kinne, S.; Kondo, Y.; Quinn, P. K.; Sarofim, M. C.; Schultz, M. G.; Schulz, M.; Venkataraman, C.; Zhang, H.; Zhang, S.; Bellouin, N.; Guttikunda, S. K.; Hopke, P. K.; Jacobson, M. Z.; Kaiser, J. W.; Klimont, Z.; Lohmann, U.; Schwarz, J. P.; Shindell, D.; Storelvmo, T.; Warren, S. G.; Zender, C. S. Bounding the Role of Black Carbon in the Climate System: A Scientific Assessment. *J. Geophys. Res. Atmospheres* **2013**, *118* (11), 5380−5552.

(9) Venkataraman, C.; Lyons, J. M.; Friedlander, S. K. Size Distributions of Polycyclic Aromatic Hydrocarbons and Elemental Carbon. 1. Sampling, Measurement Methods, and Source Characterization. *Environ. Sci. Technol.* **1994**, *28* (4), 555−562.

(10) Venkataraman, C.; Friedlander, S. K. Size Distributions of Polycyclic Aromatic Hydrocarbons and Elemental Carbon. 2. Ambient Measurements and Effects of Atmospheric Processes. *Environ. Sci. Technol.* **1994**, *28* (4), 563−572.

(11) Janssen, N. A.H.; Hoek, G.; Simic-Lawson, M.; Fischer, P.; van Bree, L.; ten Brink, H.; Keuken, M.; Atkinson, R. W.; Anderson, H. R.; Brunekreef, B.; Cassee, F. R. Black Carbon as an Additional Indicator of the Adverse Health Effects of Airborne Particles Compared with PM_{10} and $PM_{2.5}$. *Environ. Health Perspect.* **2011**, *119* (12), 1691−1699.

(12) Grahame, T. J.; Klemm, R.; Schlesinger, R. B. Public Health and Components of Particulate Matter: The Changing Assessment of Black Carbon. *J. Air Waste Manage. Assoc.* **2014**, *64* (6), 620−660.

(13) Vardoulakis, S.; Dimitrova, R.; Richards, K.; Hamlyn, D.; Camilleri, G.; Weeks, M.; Sini, J.-F.; Britter, R.; Borrego, C.; Schatzmann, M.; Moussiopoulos, N. Numerical Model Inter-Comparison for Wind Flow and Turbulence Around Single-Block Buildings. *Environ. Model. Assess.* **2011**, *16* (2), 169−181.

(14) Kumar, P.; Ketzel, M.; Vardoulakis, S.; Pirjola, L.; Britter, R. Dynamics and Dispersion Modelling of Nanoparticles from Road Traffic in the Urban Atmospheric Environment—A Review. *J. Aerosol Sci.* **2011**, *42* (9), 580−603.

(15) Tanzer, R.; Malings, C.; Hauryliuk, A.; Subramanian, R.; Presto, A. A. Demonstration of a Low-Cost Multi-Pollutant Network to Quantify Intra-Urban Spatial Variations in Air Pollutant Source Impacts and to Evaluate Environmental Justice. *Int. J. Environ. Res. Public Health* **2019**, *16* (14), 2523.

(16) Zwack, L. M.; Paciorek, C. J.; Spengler, J. D.; Levy, J. I. Modeling Spatial Patterns of Traffic-Related Air Pollutants in Complex Urban Terrain. *Environ. Health Perspect.* **2011**, *119* (6), 852−859.

(17) Apte, J. S.; Messier, K. P.; Gani, S.; Brauer, M.; Kirchstetter, T. W.; Lunden, M. M.; Marshall, J. D.; Portier, C. J.; Vermeulen, R. C. H.; Hamburg, S. P. High-Resolution Air Pollution Mapping with Google Street View Cars: Exploiting Big Data. *Environ. Sci. Technol.* **2017**, *51* (12), 6999−7008.

(18) Fujita, E. M.; Campbell, D. E.; Patrick Arnott, W.; Lau, V.; Martien, P. T. Spatial Variations of Particulate Matter and Air Toxics in Communities Adjacent to the Port of Oakland. *J. Air Waste Manage. Assoc.* **2013**, *63* (12), 1399−1411.

(19) Mueller, M. D.; Hasenfratz, D.; Saukh, O.; Fierz, M.; Hueglin, C. Statistical Modelling of Particle Number Concentration in Zurich at High Spatio-Temporal Resolution Utilizing Data from a Mobile Sensor Network. *Atmos. Environ.* **2016**, *126*, 171−181.

(20) Alexeeff, S. E.; Roy, A.; Shan, J.; Liu, X.; Messier, K.; Apte, J. S.; Portier, C.; Sidney, S.; Van Den Eeden, S. K. High-Resolution Mapping of Traffic Related Air Pollution with Google Street View Cars and Incidence of Cardiovascular Events within Neighborhoods in Oakland, CA. *Environ. Health* **2018**, *17* (1), 38.

(21) Van Den Bossche, J.; Peters, J.; Verwaeren, J.; Botteldooren, D.; Theunis, J.; De Baets, B. Mobile Monitoring for Mapping Spatial Variation in Urban Air Quality: Development and Validation of a Methodology Based on an Extensive Dataset. *Atmos. Environ.* **2015**, *105*, 148−161.

(22) Peters, J.; Theunis, J.; Poppel, M. V.; Berghmans, P. Monitoring PM_{10} and Ultrafine Particles in Urban Environments Using Mobile Measurements. *Aerosol Air Qual. Res.* **2013**, *13* (2), 509−522.

(23) Peters, J.; Van den Bossche, J.; Reggente, M.; Van Poppel, M.; De Baets, B.; Theunis, J. Cyclist Exposure to UFP and BC on Urban Routes in Antwerp, Belgium. *Atmos. Environ.* **2014**, *92*, 31−43.
(24) Kolb, C. E.; Herndon, S. C.; McManus, J. B.; Shorter, J. H.; Zahniser, M. S.; Nelson, D. D.; Jayne, J. T.; Canagaratna, M. R.; Worsnop, D. R. Mobile Laboratory with Rapid Response Instruments for Real-Time Measurements of Urban and Regional Trace Gas and Particulate Distributions and Emission Source Characteristics. *Environ. Sci. Technol.* **2004**, *38* (21), 5694−5703.
(25) Brantley, H. L.; Hagler, G. S. W.; Kimbrough, E. S.; Williams, R. W.; Mukerjee, S.; Neas, L. M. Mobile Air Monitoring Data-Processing Strategies and Effects on Spatial Air Pollution Trends. *Atmos. Meas. Tech.* **2014**, *7* (7), 2169−2183.
(26) Riley, E. A.; Banks, L.; Fintzi, J.; Gould, T. R.; Hartin, K.; Schaal, L. N.; Davey, M.; Sheppard, L.; Larson, T.; Yost, M. G.; Simpson, C. D. Multi-Pollutant Mobile Platform Measurements of Air Pollutants Adjacent to a Major Roadway. *Atmos. Environ.* **2014**, *98*, 492−499.
(27) Riley, E. A.; Schaal, L.; Sasakura, M.; Crampton, R.; Gould, T. R.; Hartin, K.; Sheppard, L.; Larson, T.; Simpson, C. D.; Yost, M. G. Correlations between Short-Term Mobile Monitoring and Long-Term Passive Sampler Measurements of Traffic-Related Air Pollution. *Atmos. Environ.* **2016**, *132*, 229−239.
(28) Adams, M. D.; Kanaroglou, P. S. Mapping Real-Time Air Pollution Health Risk for Environmental Management: Combining Mobile and Stationary Air Pollution Monitoring with Neural Network Models. *J. Environ. Manage.* **2016**, *168*, 133−141.
(29) Kerckhoffs, J.; Hoek, G.; Messier, K. P.; Brunekreef, B.; Meliefste, K.; Klompmaker, J. O.; Vermeulen, R. Comparison of Ultrafine Particle and Black Carbon Concentration Predictions from a Mobile and Short-Term Stationary Land-Use Regression Model. *Environ. Sci. Technol.* **2016**, *50* (23), 12894−12902.
(30) Larson, T. V.; Gould, T.; Riley, E. A.; Austin, E.; Fintzi, J.; Sheppard, L.; Yost, M. G.; Simpson, C. Ambient Air Quality Measurements from a Continuously Moving Mobile Platform: Estimation of Area-Wide, Fuel-Based, Mobile Source Emission Factors Using Absolute Principal Component Scores. *Atmos. Environ.* **2017**, *152*, 201−211.
(31) Shah, R. U.; Robinson, E. S.; Gu, P.; Robinson, A.; Apte, J. S.; Presto, A. A. High Spatial Resolution Mapping of Aerosol Composition and Sources in Oakland, California Using Mobile Aerosol Mass Spectrometry. *Atmos. Chem. Phys.* **2018**, *18*, 1−31.
(32) Tessum, M. W.; Larson, T.; Gould, T. R.; Simpson, C. D.; Yost, M. G.; Vedal, S. Mobile and Fixed-Site Measurements To Identify Spatial Distributions of Traffic-Related Pollution Sources in Los Angeles. *Environ. Sci. Technol.* **2018**, *52* (5), 2844−2853.
(33) Li, H. Z.; Gu, P.; Ye, Q.; Zimmerman, N.; Robinson, E. S.; Subramanian, R.; Apte, J. S.; Robinson, A. L.; Presto, A. A. Spatially Dense Air Pollutant Sampling: Implications of Spatial Variability on the Representativeness of Stationary Air Pollutant Monitors. *Atmospheric Environ. X* **2019**, *2*, 100012.
(34) Van Poppel, M.; Peters, J.; Bleux, N. Methodology for Setup and Data Processing of Mobile Air Quality Measurements to Assess the Spatial Variability of Concentrations in Urban Environments. *Environ. Pollut.* **2013**, *183*, 224−233.
(35) Miller, D. J.; Actkinson, B.; Padilla, L.; Griffin, R. J.; Moore, K.; Lewis, P. G. T.; Gardner-Frolick, R.; Craft, E.; Portier, C. J.; Hamburg, S. P.; Alvarez, R. A. Characterizing Elevated Urban Air Pollutant Spatial Patterns with Mobile Monitoring in Houston, Texas. *Environ. Sci. Technol.* **2020**, *54*, 2133.
(36) Apte, J. S.; Kirchstetter, T. W.; Reich, A. H.; Deshpande, S. J.; Kaushik, G.; Chel, A.; Marshall, J. D.; Nazaroff, W. W. Concentrations of Fine, Ultrafine, and Black Carbon Particles in Auto-Rickshaws in New Delhi, India. *Atmos. Environ.* **2011**, *45* (26), 4470−4480.
(37) Hagler, G. S. W.; Yelverton, T. L. B.; Vedantham, R.; Hansen, A. D. A.; Turner, J. R. Post-Processing Method to Reduce Noise While Preserving High Time Resolution in Aethalometer Real-Time Black Carbon Data. *Aerosol Air Qual. Res.* **2011**, *11* (5), 539−546.
(38) Patton, A. P.; Perkins, J.; Zamore, W.; Levy, J. I.; Brugge, D.; Durant, J. L. Spatial and Temporal Differences in Traffic-Related Air Pollution in Three Urban Neighborhoods near an Interstate Highway. *Atmos. Environ.* **2014**, *99*, 309−321.
(39) Tan, Y.; Robinson, A. L.; Presto, A. A. Quantifying Uncertainties in Pollutant Mapping Studies Using the Monte Carlo Method. *Atmos. Environ.* **2014**, *99*, 333−340.
(40) Caubel, J. J.; Cados, T. E.; Preble, C. V.; Kirchstetter, T. W. A Distributed Network of 100 Black Carbon Sensors for 100 Days of Air Quality Monitoring in West Oakland, California. *Environ. Sci. Technol.* **2019**, *53* (13), 7564−7573.
(41) Caubel, J. J.; Cados, T. E.; Kirchstetter, T. W. A New Black Carbon Sensor for Dense Air Quality Monitoring Networks. *Sensors* **2018**, *18* (3), 738.
(42) Messier, K. P.; Chambliss, S. E.; Gani, S.; Alvarez, R.; Brauer, M.; Choi, J. J.; Hamburg, S. P.; Kerckhoffs, J.; Lafranchi, B.; Lunden, M. M.; Marshall, J. D.; Portier, C. J.; Roy, A.; Szpiro, A. A.; Vermeulen, R. C. H.; Apte, J. S. Mapping Air Pollution with Google Street View Cars: Efficient Approaches with Mobile Monitoring and Land Use Regression. *Environ. Sci. Technol.* **2018**, *52* (21), 12563−12572.
(43) Hansen, A. D. A.; Rosen, H.; Novakov, T. The Aethalometer — An Instrument for the Real-Time Measurement of Optical Absorption by Aerosol Particles. *Sci. Total Environ.* **1984**, *36*, 191−196.
(44) Grubbs, F. E. On Estimating Precision of Measuring Instruments and Product Variability. *J. Am. Stat. Assoc.* **1948**, *43* (242), 243−264.
(45) Arnott, W. P.; Moosmüller, H.; Sheridan, P. J.; Ogren, J. A.; Raspet, R.; Slaton, W. V.; Hand, J. L.; Kreidenweis, S. M.; Collett, J. L. Photoacoustic and Filter-Based Ambient Aerosol Light Absorption Measurements: Instrument Comparisons and the Role of Relative Humidity. *J. Geophys. Res.* **2003**, *108* (D1), AAC 15−1−AAC 15−11.
(46) Tasoglou, A.; Subramanian, R.; Pandis, S. N. An Inter-Comparison of Black-Carbon-Related Instruments in a Laboratory Study of Biomass Burning Aerosol. *Aerosol Sci. Technol.* **2018**, *52* (11), 1320−1331.

https://dx.doi.org/10.1021/acs.est.0c01409
Environ. Sci. Technol. 2020, 54, 7848−7857